Open Ceramics 7 (2021) 100167

Contents lists available at ScienceDirect

Open Ceramics

journal homepage: www.sciencedirect.com/journal/open-ceramics

Development of calcium phosphate suspensions suitable for the stereolithography process

Chloé Goutagny [a], Stéphane Hocquet [a,*], Dominique Hautcoeur [a], Marie Lasgorceix [b], Nicolas Somers [b], Anne Leriche [b]

[a] Belgian Ceramic Research Center (BCRC), Mons, Belgium
[b] Univ. Polytechnique Hauts-de-France, EA 2443 - LMCPA - Laboratoire des Matériaux Céramiques et Procédés Associés, F59313, Valenciennes, France

ARTICLE INFO

Keywords:
Stereolithography
Tricalcium phosphate
Resin formulation
Polyacrylates
Debinding
Thermal degradation

ABSTRACT

With the median age of the population steadily rising, the rate of bone disorders increases as well, making the need of bone implants more and more urgent in our society. However, manufacturing of synthetic bioimplants requires high flexibility of the process and materials with sufficient mechanical strength and biocompatible properties. This paper is devoted to the printing of β-tricalcium phosphate (β-TCP) by stereolithography. The suspensions or pastes containing the photosensitive-resin mixed with β-TCP powder were assessed for the following parameters: rheological behaviour, thermal degradation of photo-cured samples, quality of green and sintered parts. It appeared that the composition of the photo-sensitive resin influences the viscosity of the paste. However, no direct correlation could be drawn between the viscosity of the photo-sensitive resins and the viscosity of the whole paste. A hypothesis is that the chemical structure of the monomers composing the photo-sensitive resin also impacts the viscosity of the paste. A thermal debinding cycle was built from the thermogravimetric analysis of the photo-cured samples. The structure of the post printed (green) parts and final parts (parts after debinding and sintering) was evaluated. It appeared that the pastes with the lowest viscosity were the easiest to process, and that the green parts made with these pastes were the easiest to clean, reducing the number of defects in the sintered parts. Process optimisation was also assessed. Different light parameters were evaluated, and it appeared that reducing the light power during the printing improved the resolution as well as the quality of the sintered parts.

1. Introduction

Additive manufacturing of ceramics is used as an alternative to other conventional processes and allows the fast production of objects with complex shapes [1]. Stereolithography (SLA), enabling the printing of a green object through the layer by layer photo-polymerisation of a ceramic loaded photosensitive paste, is one of the technologies providing the best accuracy and resolution [2]. Considering the increased need of bone implants due to the rising median age of the population [3], the SLA process, applied to bio-ceramic parts manufacturing for custom-made implants, is of great interest in the orthopaedic field.

Concerning the materials, Hydroxyapatite (HA) and β-tricalcium phosphate (β-TCP) appear both as materials of choice for bone implants: they are stable and their apatitic structure and chemical composition is close to the mineral part of bones [4], making them compatible to the human body [5]. Moreover, the osteoconductive quality of both materials allows the guiding and remodelling process of natural bone growth. However, while β-TCP is bioresorbable (i.e. it rapidly dissolves in the human body as the new bone reforms) due to its low dissolution rate [6], HA does not have that quality.

Consequently, using SLA with either HA or β-TCP powders could provide objects with complex geometries, good stability and biocompatibility [4,5]. In SLA process, photo-sensitive resin composed of monomers and a photo-initiator are mixed to ceramic powder to prepare pastes with adequate rheological properties. However, currently very few pastes containing calcium phosphate materials are available on the market, and most of the parts made with these pastes via SLA still present many defects such as cracks and delaminations [7]. Nonetheless, the production of macro-porous parts with a sufficient mechanical stability for some applications is possible for some commercial pastes [8].

The green parts, obtained at the end of the printing with an SLA

* Corresponding author. Stéphane Hocquet. , Avenue du gouverneur Cornez 4, 7000, Mons, Belgium.
E-mail address: S.hocquet@bcrc.be (S. Hocquet).

https://doi.org/10.1016/j.oceram.2021.100167
Received 27 January 2021; Received in revised form 29 July 2021; Accepted 30 July 2021
Available online 11 August 2021

machine, are composed of two materials: the ceramic powder and the photo-polymerized resin (in which the ceramic powder is trapped). Debinding and sintering steps are therefore necessary to obtain dense and pure ceramic parts. Several studies show that the debinding is the most critical step of the process [9,10]. Indeed, the removal of the photopolymer network either by decomposition or evaporation during the debinding step generates a lot of pressure in the parts, causing cracks and delamination. In order to avoid the appearance of such defects, different options have been considered, the optimisation of the composition of the resin being one of them. However, there are numerous criteria needed for a paste to be printable: a low viscosity at low shear rate, in the range of 5–10 Pa s for shear rates between 0 and $300s^{-1}$ [11], a shear-thinning behaviour [9,10], 13], and a sufficient light reactivity providing a strong polymer network and adhesion between each layer [2,14].

The viscosity of the pastes is influenced by two factors: the composition of the photo-sensitive resin and the solid loading [9]. Moreover, in order to obtain a shear thinning behaviour, a dispersant is needed to prevent the powder from agglomerating, causing an unwanted shear-thickening effect [15]. The adhesion between the layers is determined by the cure depth, which depends on the following parameters: the nature of the photo-initiator, its concentration, the energy dose given by the machine, the reactivity of the resin, the amount of powder, its refractive index and its colour [16].

Acrylates, due to their high penetration depth [7,17–19], are the monomers often used for the resin formulation needed in SLA. There are two main types of SLA machines depending on their light source: machines operating with a laser [20] and machines using a dynamic light projector (DLP) [21]. In this work, emphasis will be given to the machines working with a DLP.

The obtaining of an effective cure [22] of the photo-sensitive resin depends on an overlap between the emission spectrum of the light source and the absorption spectrum of the photo-initiator. For example diphenyl (2,3,4-trimethylbenzoyl) phosphine oxide (TPO) and (2,3,4-trimethybenzoyl) phosphine oxide (BAPO) are often chosen when working with light around 405 nm [23–25]; whereas the 2,2-dimethoxy-1,2-phenylethan-1-one (DMTPA) which absorbs in the range of 220–380 nm is chosen for a light of 355 nm [16].

Information on the composition of the pastes, in particular concerning the formulation of the resin, is generally absent from the literature. The objective of this work is to give an overview on the possible resin composition and the influence of each component on the rheological behaviour of the paste, its printability and the thermal degradation of the green parts. Moreover, the cleaning of the parts is also shortly assessed, and the microstructure and density of the final objects is evaluated.

2. Materials and methods

2.1. Raw materials for the ceramic paste

The β-TCP powder was synthesised through aqueous precipitation from di-ammonium phosphate solution ($(NH_4)_2HPO_4$, 98.0–102.0%, Carlo Erba, France) added to calcium nitrate solution ($Ca(NO_3)_2{\cdot}4H_2O$ > 98.0%, Honeywell, Germany) inside a double-wall reactor. This method is well-known and documented in the literature [26]. The addition speed of the $(NH_4)_2HPO_4$solution, pH and temperature were controlled throughout the whole process. The pH was kept at 6.7 using ammonium hydroxide (NH_4OH 30%, Carlo Erba, France) and the temperature fixed at 31 °C. The extracted precipitate was filtered, dried and calcined at 850 °C during 3 h. The raw powder, obtained after calcination, presents a density of 3.07 g cm^3. The mineralogical composition of the produced powder, as well as the sintered parts, were evaluated with X-Ray Diffraction (XRD) using a diffractometer RIGAKU Miniflex 600. Measurements were performed for θ angles between 20 and 60° as described in the literature for β-TCP [27,28].

The chosen photo-initiator for this study, diphenyl (2,3,4-trimethylbenzoyl) phosphine oxide (TPO), was purchased from Sigma Aldrich. For the photosensitive resin, five acrylate monomers were also purchased from Sigma Aldrich: two diacrylates (1,6-hexanediol diacrylate, HDDA) and tetraethylene glycol diacrylate, TGDA)), one triacrylate (Trimethylopropane trimethacrylate, TTA)) and one methacrylate (2-hydroxyethylmethacrylate, HEMA)). The molecular weight of these chosen monomers are: $M_{nPEGDA} = 575.0$, $M_{nTTA} = 338.4$, $M_{nTGDA} = 302.3$, $M_{nHDDA} = 226.3$, $M_{nHEMA} = 130.1$. Polyethylene glycol 200 (PEG 200, Sigma Aldrich) was added as a non-reactive diluent and a phosphate ester (Zelec P312, Sepan Europe), was used as a dispersant.

2.2. Preparation of pastes

The two components of the paste (the photo-sensitive resins and the powder) were prepared separately before being mixed.

The photo-sensitive resins were prepared by mixing together, in an opaque container, monomers and the photo-initiator during 2 h with rotary mixer. The photo-initiator was added in a concentration of 1 wt% to the monomers weight.

To avoid the formation of agglomerates during the mixing of the powder and the photo-sensitive resins, a pre-coating of the powder with a dispersant was carried out. Amounts of dispersant in the range of 0.2 to 2 wt% of the powder were tested. The coating of the dispersant around powder particles was achieved as follows: the dispersant was added in an ethanol suspension containing 50 wt% of β-TCP powder. Subsequently, ball milling of the suspension was achieved using 2 mm diameter zirconia beads overnight in a rotary mixer. The ethanol was then removed by evaporation at 80 °C, and the coated powder was dried at 105 °C. During this process, the dispersant is adsorbed around the particles, providing both steric and electric repulsion between the particles once the powder was mixed with the resin [18]. This repulsion avoids agglomeration, reduces the viscosity of the paste and enables a higher solid load.

The goal set in this work was to have printable pastes made with at least 47 vol% of powder in order to obtain high green density and consequently improve the densification during the sintering process. The coated powder was added progressively in the resin and mixed in a rotary mixer with 1 cm diameter zirconia beads (to homogenise the paste) during 1 h. The advantage of using 1 cm diameter zirconia beads is that the mixing of the powder in the photo-sensitive resin was improved and that they can easily be removed after the process. The as-obtained paste went through a three-roll mill to improve its homogeneity and eliminate the agglomerates.

2.3. Printing with the stereolithography technique

Parts were shaped with an SLA machine working with a dynamic light projector (DLP) (Admaflex 130, Admatec Europe, NL). The DLP uses LEDs to project light at 405 nm and enables the curing of the whole layer at once. The resolution of the machine is 2560 × 1600px for an area of 135 × 85 mm. The machine combines the tape casting technique with SLA. The paste is placed in a reservoir and a thin layer of paste is cast on a plastic film as it moves under a doctor blade. Then, the building platform goes down to the wanted layer thickness and the light is projected from below the film, enabling the curing of the paste. The remaining uncured paste is pumped back with a wiper seal and a peristaltic pump into the reservoir to avoid waste. The light parameters such as LED power, given as a percentage of the maximum power of the projector, and exposure time were modified to evaluate their effect.

The tape casting technology presents the advantage to prevent the parts from being in a vat surrounded by uncured material. It allows the easy recovering at the end of the printing and reduces the cleaning thanks to the absence of uncured material around the parts during the process.

To avoid the formation of defects in the parts (Fig. 1), a

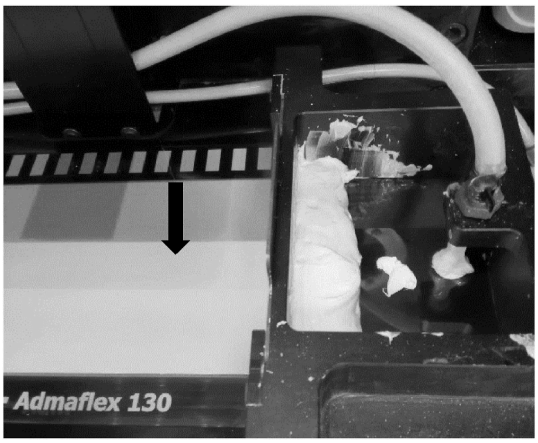

Fig. 1. Example of a homogeneous layer of a suspension loaded with 48 vol% of β-TCP (black arrow) spread on the film in an Admaflex 130 machine. Reservoir on the right of the image with the tube connecting it to the slurry wiper (not shown here).

homogeneous layer of paste on the film is required. This means that in order to achieve a homogeneous recoating with the tape-casting process [11,12] and avoid leaking below the doctor blade, the paste's rheological behaviour should be shear-thinning and its viscosity in the range of 5–10 Pa s at low shear rates (below $300s^{-1}$) [29]. Consequently, the printability of the paste has to be evaluated in the light of its viscosity and the appearance of the layer spread on the film.

Two designs were selected to begin the printing tests: a microporous cube, 12 mm side with 2.4 mm holes and a pellet of 12 mm diameter and 3 mm thickness. The cube was chosen in order to evaluate the resolution by looking at the size and definition of the holes. The pellet was chosen to easily measure the density of sintered samples.

After the printing process, the parts were removed from the platform and cleaned with ethanol which enabled the cleaning of the uncured paste without damaging the samples. Two cleaning methods for the removing of the uncured paste in the printed parts were tested: in the first method, the parts were cleaned with ethanol directly after printing, dried and left at room temperature. In the second method, the parts were immersed in ethanol and placed in an ultrasonic bath before being dried and left at room temperature.

Then, the cleaned parts were debinded and sintered according to the cycle presented in Fig. 2, deduced from the thermogravimetric analysis discussed in part 4.

2.4. Characterizations

The rheological behaviour was studied with a Haake Mars III rheometer (ThermoFisher Scientific), using a cone plate 1° configuration, in rotation mode at a regulated temperature of 22 °C for shear rate in the range of 0 to $600s^{-1}$ in 600 s. Then $600s^{-1}$ was held for 30 s and finally the shear rate went back to $0s^{-1}$ in 600 s.

The thermal degradation of the different cured resins in the green parts was controlled by thermogravimetric analysis (TGA, LINSEIS) in air (100 ml/min) between 25 °C and 550 °C with a temperature ramp of 10 °C/min.

The photo-polymerisation thickness was determined by illuminating a layer without any building platform and by measuring the cured sample with a calliper.

Illumination tests were performed on both the resin alone and on the paste. The tested material was put on a transparent plastic film, placed on the machine and illuminated with the projector at the chosen light parameters. For the first trials, the light parameters were 85% of light power during 2.5s, before being adapted to each paste. In order to estimate the reactivity of the resins, the uncured resin was weighted before illumination and the cured part of the resin was weighted after illumination. The photo-polymerisation rate was estimated by comparing the initial mass of the resin to the mass of the cured sample. The conversion rate was calculated as (Eq. (1)):

$$Converstion\ rate = \frac{Mass\ of\ the\ cured\ sample}{Initial\ mass\ of\ the\ resin} \quad (1)$$

The Archimedes' principle was used to determine the open porosity of sintered samples. The samples were dried in an oven at 105 °C overnight before measurements. The samples were placed under water during 2 h in a vacuum bell jar, then vacuum (around 2 kPa) was held for 2 h. Directly after, the samples were weighed, first under water, then under air to establish the wet mass.

The surface quality and the microstructure of the green and sintered samples were evaluated using an optical microscope and low vacuum (<10 mPa) scanning electron microscopy (SEM) (JCM-6000 JEOL Europe). Samples have been coated with platinum under vacuum using an evaporating system JEOL JFC-1300 before SEM observations.

3. Results

3.1. Reactivity and rheological behaviour of the resin components

When mixed with 1 wt% of photo-initiator and illuminated at 85% of LED power during 2.5s, the various tested acrylates monomers presented different photo-polymerisation rates assimilated here to the conversion rates (Table 1). Observations were also made on the texture of the samples. The experiment was conducted 3 times and an average of the mass was calculated. The collected data are presented in Table 1.

In order to provide mechanical stability to the green part, the resin must have sufficient reactivity and lead to a strong photopolymer network. The reactivity of the resin depends on the number of functional

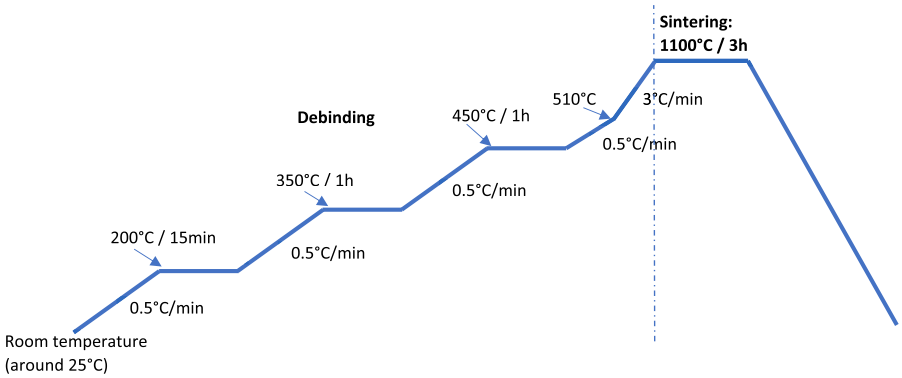

Fig. 2. Debinding and sintering cycle under air for β-TCP parts printed with the Admafex 130 machine.

Table 1
Evaluation of the reactivity of the monomers mixed with 1 wt% (of the monomer weight) of diphenyl (2,3,4-trimethylbenzoyl) phosphine oxide (TPO). 1 g of each resin was illuminated at 85% of LED power during 2500 ms.

TGDA Mn = 302.3	HDDA Mn = 226.3	TTA Mn = 338.4	HEMA Mn = 130.1	TPO (g)	Conversion rate (%) (±0.10%)	Texture
100%				1%	0.65	Hard sample
	100%			1%	0.59	Hard sample
		100%		1%	0.78	Soft and friable sample
			100%	1%	0	No sample

groups in the monomers, its viscosity and the light curing parameters of the machine.

The TTA proved to be the monomer with the highest conversion rate under these experimental conditions. However, TGDA and HDDA were the monomers that provided the hardest samples, whereas TTA led to soft and friable samples. Finally, HEMA did not polymerise in the conditions of this experiment.

The reactivity of the monomers and their viscosity are intrinsically linked [30], therefore the viscosity of each monomer was evaluated. The results, presented in Fig. 3, showed that all the monomers have a Newtonian behaviour, their viscosity does not depend on the shear rate and can be determined using the slope of the lines: the higher the slope, the higher the viscosity [31].

The TTA is the acrylate monomer with the highest viscosity. HDDA and HEMA are the monomers with the lowest viscosity.

Tables 2 and 3 show the results of a second photo-polymerisation test that was done on mixtures of monomers. Considering that TGDA led to hard samples and presented a low viscosity compared to TTA, it was chosen as the main component of the mixtures. For this test, two sets of light parameters were chosen: 85% of LED power during 2.5 ms (Table 2) and 50% of LED power during 1.5s (Table 3).

As shown in the tables, the light parameters of 85% of LED power and 2.5s of exposure time led to higher conversion rates for all the tested resin mixtures. For these illumination conditions, the differentiation between samples was difficult.

On the other hand, with the light parameters 50% of LED power and 1.5s of exposure time, it appeared that all the resins prepared with TTA

Table 2
Reactivity of mixtures of monomers with 1 wt% of TPO and illuminated at 85% of light power during 2500 ms.

	TGDA	HDDA	TTA	PEG	TPO	Conversion rate (±0.10%)
1	90%	10%			1%	0.95
2	70%	10%	20%		1%	0.90
3	75%	8%		17%	1%	1,00
4	58%	8%	17%	17%	1%	0.85
5	55%	9%	18%	18%	1%	0.90

Table 3
Reactivity of mixtures of monomers with 1 wt% of TPO and illuminated at 50% of light power during 1500 ms.

	TGDA	HDDA	TTA	PEG	TPO	Conversion rate (±0.10%)
1	90%	10%			1%	0.75
2	70%	10%	20%		1%	0.50
3	75%	8%		17%	1%	0.95
4	58%	8%	17%	17%	1%	0.50
5	55%	9%	18%	18%	1%	0.50

(2, 4 and 5) led to the same conversion rate: 0.5%, that was also the lowest conversion rate. Considering that a high mechanical strength is needed for the green part, therefore the TTA does not appear as a good choice for the resin composition to prepare paste.

The resin with the highest conversion rate is the resin 3 containing TGDA HDDA and PEG 200. The resin 1 containing only TGDA and HDDA has a lower conversion rate than the resin 3, therefore PEG 200 appeared to be an interesting additive.

3.2. Printability of ceramic paste

Using a mixture of TGDA (as the main component), HDDA (as the co-monomer with the lowest viscosity), and PEG 200 (as the non-reactive diluent), pastes with 47 vol% (around 71 wt%) of β-TCP powder were prepared with different quantities of dispersant from 0.2 to 0.7 wt% of the β-TCP powder.

The paste prepared with 0.2 wt% of dispersant presented a clear shear-thickening behaviour after mixing, with high agglomeration, disqualifying this paste from further rheological analysis.

The viscosity of the various pastes measured at 100 and 200s^{-1} are presented in Fig. 4. For the three pastes, the viscosity was lower at the highest shear rate: 200s^{-1} and the lowest viscosity values for both shear

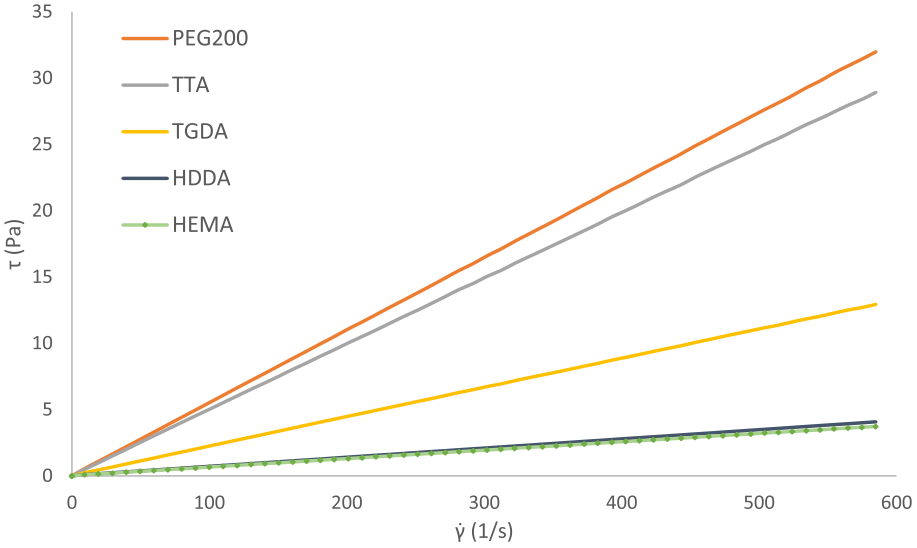

Fig. 3. Rheological behaviour of the monomers (shear stress (τ) versus shear rate (γ̇)).

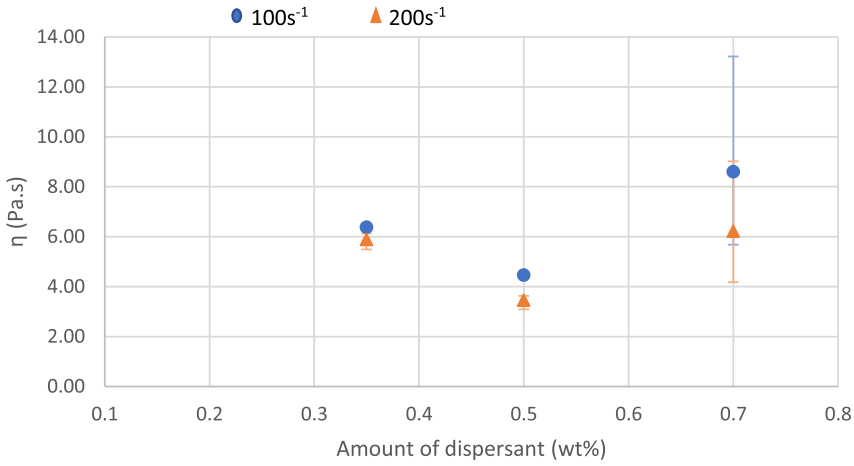

Fig. 4. Viscosities (Pa.s) of pastes, prepared with similar resins containing TGDA, HDDA and PEG 200 and loaded with 47 vol% of β-TCP powders containing different amount of phosphate ester dispersant, at different shear rates.100s^{-1} 200s^{-1}..

rates corresponded to 0.5 wt% of dispersant. Therefore, this amount of dispersant was chosen to conduct the remainder of the experiments.

Nine photo-sensitive resins were prepared with the selected monomers: TGDA, HDDA, TTA, HEMA and PEG 200, and their viscosities were measured between 0 and 600s^{-1}. The photo-sensitive resins are also Newtonian fluids, their average viscosity was calculated and reported in Table 4. The mixture of different monomers allowed the covering of a range of viscosity from 22 to 12 mPa s.

Pastes with 47 vol% of powder were prepared from these resins, their composition is reported in Table 4. The viscosity of each paste was measured between 0 and 600s^{-1}, the shear stress versus the shear rate is plotted in Fig. 5. The rheological behaviour of the pastes was not Newtonian, their viscosity depended on the shear rates, therefore it was not possible to obtain an average viscosity but in order to facilitate the comparison between the pastes, the dynamic viscosity of each paste was measured at the specific shear rate of 100s^{-1} and reported in Table 4.

It was not possible to prepare homogeneous pastes with the two samples having the higher viscosity, i.e. sample resins R1 and R2. Consequently, their rheological behaviour could not be evaluated.

The viscosities of the pastes at 100s^{-1} were between 3.5 and 7.6 Pa s. However, no obvious correlation between the resins viscosities and the pastes viscosities could be established. Indeed, the classification of the pastes using their viscosity from the lowest viscosity to the highest is as follows: S6 < S7 < S4 < S9 < S8 < S3 < S5, whereas the classification of the pastes using the resins viscosities from the lowest to the highest is different: S3 < S4 < S5 and S6 < S8 < S7 and 9.

For the pastes S5, S3, S8 and S7, the evaluation of the rheological behaviour became impossible up to 600s^{-1}, as their too high viscosity at high shear rates made the measurements with this configuration inaccurate.

The viscosity versus shear rate of the pastes with the lowest viscosities was plotted in Fig. 6. The decrease of their viscosity with the increase of the shear rate showed their shear-thinning behaviour. Moreover, for shear rates from 20 to 600s^{-1}, the viscosity of the pastes was below 10 Pa s which is the suitable viscosity for SLA printing with tape-casting [11].

3.3. Thermal degradation patterns depending on the polymeric phase

The impact of the resin composition on the thermal degradation was studied with the pastes S1, S3, S6 and S7. Cured samples of each paste for the thermogravimetric analysis were obtained by illuminating few ml of the paste spread onto the plastic film of the SLA device. Thermogravimetric curves of the cured samples corresponding to the pastes S1, S3 and S6 are presented in Fig. 7.

Two samples were cured from the suspension S7 with two sets of light parameters to check the influence of the LED power on the thermal degradation of the photopolymer network:

- LED power = 70%; exposure time = 4.5s (a)
- LED power = 50%; exposure time = 4.5s (b)

The thermogravimetric analysis of the cured samples are presented in Fig. 8.

For the paste S1 (48 vol% of β-TCP powder with 0.5 wt% of dispersant, TGDA and 1 wt% of TPO), the weight loss started around 250 °C and was brutal up to 400 °C, where a small slowdown was observable. The organic phase was completely eliminated after 470 °C.

For the paste S3 (48 vol% of β-TCP powder with 0.5 wt% of dispersant, TGDA, HDDA and 1 wt% of TPO), the mass loss began slowly at

Table 4
Resin and corresponding paste rheological measurements at 100 s^{-1}.

Resins	TGDA (R1)	R2	R3	R4	R5	R6	R8	R7	R9
Resins' viscosity (Pa. s) (±0.0001)	0.022	0 .022	0.017	0.016	0.015	0.015	0.013	0.012	0.012
Resins' composition (wt%)	TGDA	85%TGDA 5% HEMA 10%PEG 200	80%TGDA 20%HDDA	60%TGDA 30%HDDA 10%PEG 200	70%TGDA 30%HDDA	50%TGDA 40%HDDA 10%PEG 200	60%TGDA 40%HEMA	40%TGDA 35% HDDA 15%HEMA 10%PEG 200	55%TGDA 45%HDDA
Pastes	S1	S2	S3	S4	S5	S6	S8	S7	S9
Pastes' viscosity at 100 s^{-1} (Pa s) (±0.4)	Non measurable	Non measurable	7.0	4.4	7.6	3.5	5.8	3.8	4.5

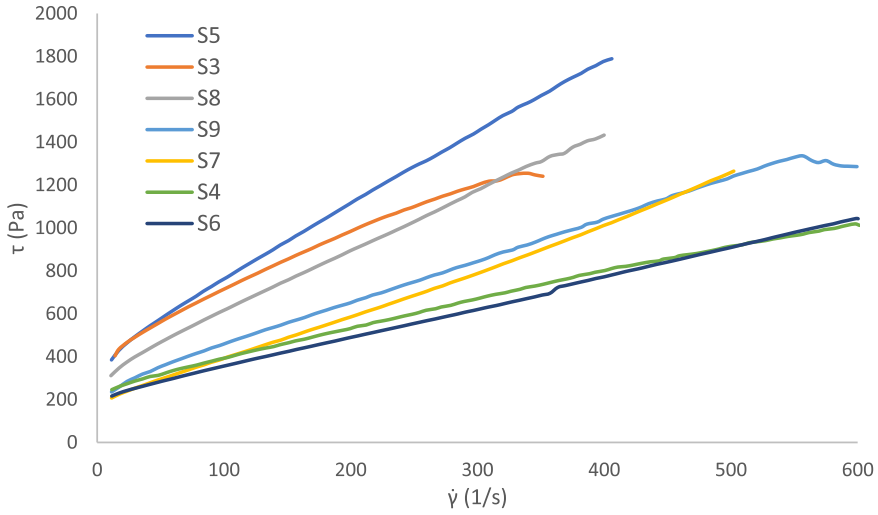

Fig. 5. Rheological behaviour (shear stress (τ) versus shear rate (γ̇)) of suspensions made from different resins (resin's composition are given in Table 3) the measurements were carried three times and an average curve was plotted (standard deviation± 0.4 Pa s).

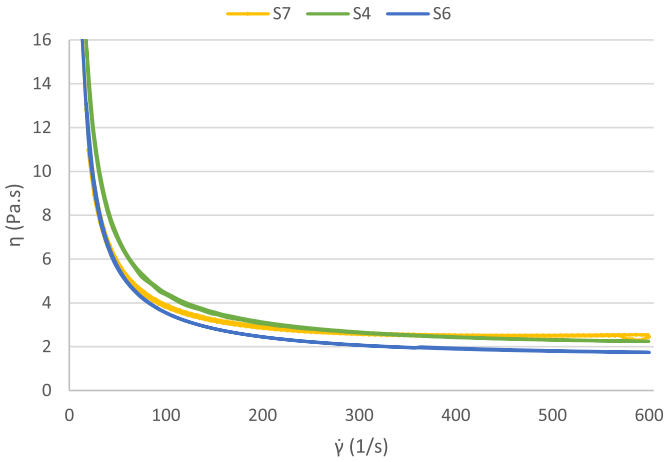

Fig. 6. Viscosity versus shear rate for the suspensions (loaded with 47 vol% of powder) with the lowest viscosities (the measurements were carried three time and an average curve was plotted).

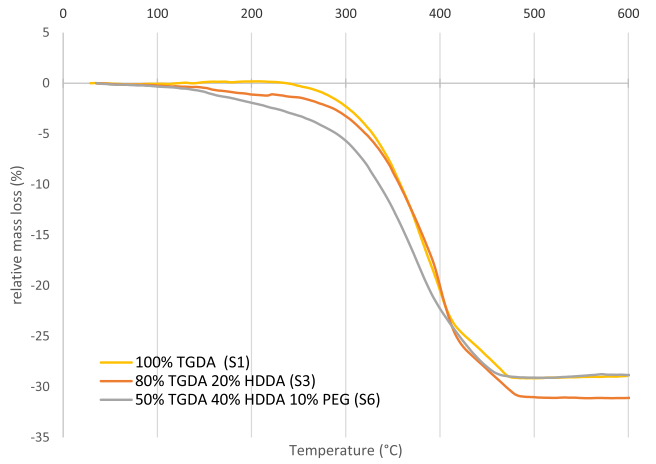

Fig. 7. Thermogravimetric analysis of cured suspension S1, S3 and S6 prepared with different resins: S1 = 100%TGDA, S3 = 80%TGDA 20%HDDA, S6 = 50% TGDA 40% HDDA 10%PEG and illuminated at 85% of LED power during 2.5s.

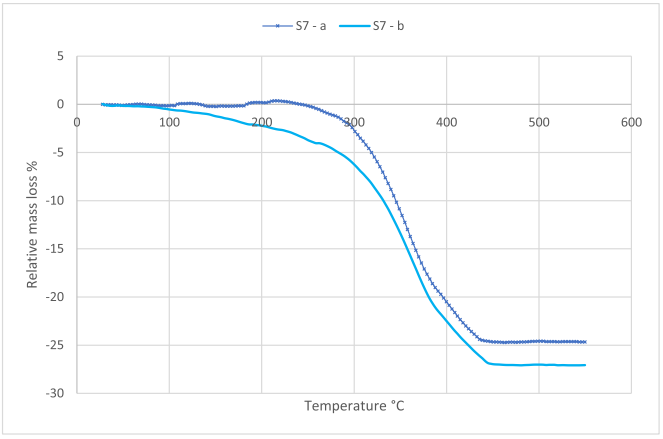

Fig. 8. Thermogravimetric analysis of cured suspension made with 40%TGDA 35%HDDA 15%HEMA and 10%PEG 200 (S10) illuminated at 50% of LED power during 4.5s and 70% of LED power during 4.5s.

100 °C before dropping brutally at 320 °C and slowing down again around 400 °C. The mass loss stopped after 490 °C.

For the paste S6 (48 vol% of β-TCP powder with 0.5 wt% of dispersant, TGDA, HDDA, PEG 200 and 1 wt% of TPO), the mass loss started slowly around 80 °C before dropping brutally around 320 °C. Then the thermal degradation pattern was similar to the one observed for S3.

The sample illuminated with the highest light power (a) showed no sign of thermal degradation before 250 °C, whereas for the parts illuminated with lower LED power (b) the thermal degradation began around 90 °C. Moreover, for the sample illuminated with the lowest LED power (b) at 250 °C, 3.7 wt% of photopolymer had already been eliminated.

3.4. Drying, debinding sintering and characterization of the final parts

The designs selected for the printing tests (mentioned in point 2.3) are represented in Fig. 9.

Considering the previous results (Table 4, Figs. 5 and 6), the pastes S6 and S7 were the ones with the lowest viscosities. Such viscosities enabled a homogenous spread of the pastes onto the plastic film of the SLA machine. Therefore, pastes with the same compositions were prepared and used for the printing tests. The composition of the resins is

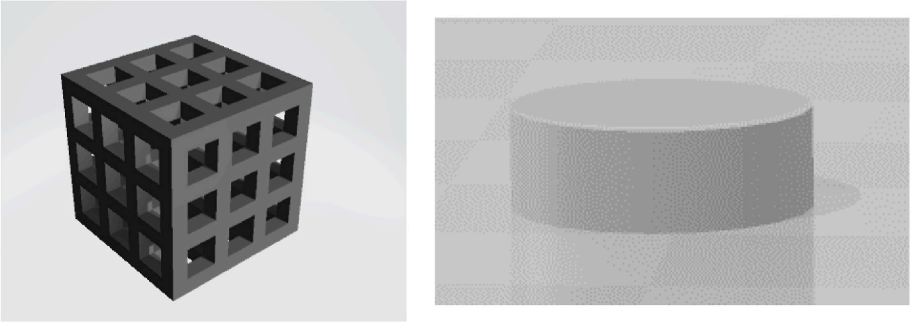

Fig. 9. 3D files, 10 mm length cube, 3 mm thickness and 12 mm diameter pellet.

reminded in Table 5 and the light parameters used to print the parts are presented in Table 6.

Microscopic images of the printed parts I1 to I4 are presented in Fig. 9. I1 (A) presented a poor resolution: the holes were smaller than the ones on the original 3D design, there was a lot of overcuring and some of the holes were obstructed. A better resolution with square-shaped holes that were not obstructed has been observed for I2 (B), but a lot of overcuring made them smaller than the ones on the 3D design. I3 (C) presented the worst resolution: all the holes were obstructed and not square-shaped. Moreover, I3 was not finalized, as the part dropped during the printing process; considering the very poor resolution of this part, this experiment was not reconducted. I4 (D) presented the best resolution with square shaped and unobstructed holes.

The removal of the excessive uncured material is an important step in the cleaning process, especially in microporous structures where uncured paste can obstruct the holes [18]. Two cleaning methods with ethanol were tested: with and without sonication. The pellet cleaned with sonication (Fig. 11) showed small impacts on its surface; this effect did not occur on the part cleaned without sonication (Fig. 12).

After cleaning the parts, the cured polymer was removed by thermal debinding and the ceramic scaffolds obtained were sintered following the thermal cycle presented in Fig. 2. The sintered scaffolds are presented in Fig. 10.

I2 (B) and I4 (D) appeared to be the parts with the least number of defects after thermal treatment. I1 (A) and I3 (C) presented large cracks and delamination.

SEM analysis was performed on one of the sides of each sample (Fig. 14). The micrographs are presented in Fig. 15.

On the SEM micrograph of sample I1 (A), many defects are visible (highlighted with red arrows and circle): the printed layers formed a "stair"-like pattern on the surface. The same observation has been made for sample I2 (B), but with larger pores. Samples I3 (C) and I4 (D) presented a smoother surface compared to I1 and I2.

Five pellets printed at 45% of LED power during 3s, with a resin composed of 50%TDGA, 40%HDDA, 10%PEG and 47 vol% of β-TCP powder, were debound and sintered following the cycle presented in Fig. 2. Their apparent density is presented in Table 5. XRD diffractogram of the sintered part, presented in Fig. 16, was compared to ICCD file of β-TCP phase and revealed the presence of only β-TCP.

4. Discussion

The first step towards the preparation of suitable pastes for the SLA was the study of the photosensitive resins alone. The choice of the monomers and the photo initiator influences the resins properties in terms of reactivity and viscosity. Indeed, the results presented in Table 1 showed that, for the same light parameters, different monomers led to different photopolymerised samples. Based on the results found in the literature, these observations can be explained considering two different aspects of the reactivity of the resin. On the one hand, the functionality of the monomer has its importance; it has been shown that acrylates are more reactive than methacrylates [32,33], which explains why the HEMA did not photopolymerise. On the other hand, the viscosity of the monomers influences the mobility of the reactive species and therefore impacts the reactivity of the photo-sensitive resin; a high viscosity slows down the diffusion of the reactive radicals and therefore reduces the photopolymerisation rate [33].

However, the experiments carried out with the monomers TGDA, HDDA, TTA and HEMA alone seemed to be in contradiction with this explanation. Indeed, the heaviest photopolymerised sample (i.e. the sample with the highest conversion rate) was obtained with TTA, the most viscous monomer (Fig. 3). The low viscosity of TGDA and HDDA, associated with their high reactivity at the light parameters chosen, led to a very fast photo-polymerisation and should have given the highest conversion rates which is not the case in our study. Their lower conversion rates could be explained considering that reactive radicals have been trapped inside the solidified network, causing the reaction to stop before the whole resin was cured.

However, the negative impact of a high viscosity on the resin reactivity is observable with the experiments conducted on mixtures of monomers illuminated at 50% during 1.5s (Table 4) and is in correlation with the data found in the literature [33]. In this case, the resins 2, 4 and 5 prepared with TTA (the most viscous monomer) led to lighter samples than the resins 1 and 3 (least viscous resins). Here, the propagation reaction of the photo-polymerisation is diffusion-limited, therefore more viscous resins led to lower conversion rates [33].

The experiments conducted on mixtures of monomers also showed that the reactivity of the monomers depends on the light parameters used. Higher light parameters (85% of LED power during 2.5s) led for all the prepared resins to heavier samples (Tables 3 and 4). Consequently, the application of a higher energy dose can lead to a higher degree of conversion of the monomers in the resin [16,34] therefore leading to

Table 5
Resin composition of parts printed with pastes loaded with 48%vol of β-TCP powder with 0.5 wt% of dispersant.

Parts	TGDA (wt%)	HDDA (wt%)	PEG 200 (wt%)	HEMA (wt%)
I1 and I2	50	40	10	
I3 and I4	40	35	10	15

Table 6
Light parameters used to print the parts with suspensions containing 48 vol% of β-TCP and a resin made of 50% of TGDA, 40% of HDDA and 10% of PEG 200 for parts I1; and I2 and 40% of TGDA, 35% of HDDA, 10% of PEG 200 and 15% of HEMA for parts I3 and I4.

Parts	Light power (%)	Exposure time (ms)
I1	55	2000
I2	35	2000
I3	55	4500
I4	45	3000

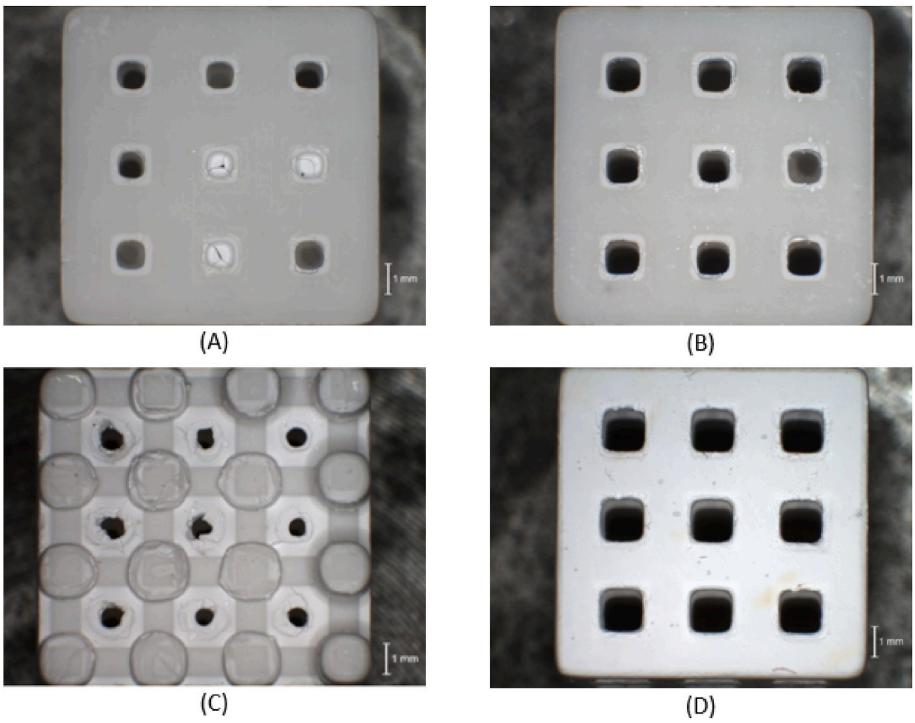

Fig. 10. Green parts I1 (A) illuminated with 55% of LED power during 2s, I2 (B) illuminated with 35% of LED power during 2s, I3 (C) illuminated with 55% of LED power during 4.5s, I4 (D) illuminated with 45% of LED power during 3s.

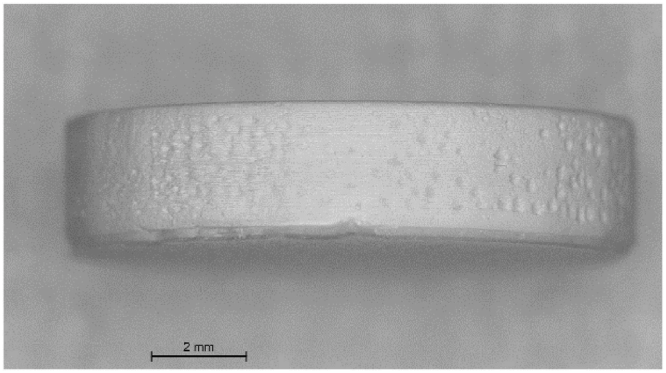

Fig. 11. Pellet cleaned only with ethanol.

Fig. 12. Pellet cleaned with ethanol in an ultrasonic bath.

higher conversion rates.

The differences between the cured samples, depending on the resin composition and the light parameters, seemed also to have an impact on the printed samples characteristics. In Figs. 9, 13 and 14, parts I1 (A) and I3 (C) were printed with the same light parameters but with different compositions. Part I1 presented more defects and a rougher surface than part I3. This could be explained by the presence of HEMA in the resin of part I3, which could reduce the reactivity (as observed in Tables 2 and 3) and therefore slow down the reaching of the gelation point, leading to a poor layer integration and poor resolution [25]. A similar conclusion can be made when comparing parts printed with the same composition but different light parameters. Indeed, in Fig. 9, parts I2 (B) and I4 (D), printed with the lowest energy rate, had a better resolution than parts I1 and I3. In this case the photo-polymerisation rate was governed by the energy dose [16].

Moreover, the resin composition and its viscosity also influence the viscosity of the pastes and therefore their processability. Table 4 showed that, with a viscosity above 20 mPa s, it was not possible to obtain a printable paste, but no correlation was found between the resin viscosity and the paste viscosity. The same observation was done by Badev et al. [35] who showed that the addition of a small quantity of HDDA to the amine modified polyether acrylate (main component of the resin) reduced its viscosity, but not the global viscosity of the paste. Even though no correlation was found between the resin viscosity and the paste viscosity, it appears in Table 3 that depending on the resin composition, the viscosity of the paste is not the same. A hypothesis to explain that would be that the resin composition influences the interaction between the monomers, the dispersant and the particles, and therefore influences the global viscosity of the paste.

Experiments have shown that the more the viscosity of the paste increased the more the printed layer could be stuck to the tape casting film which could induce stress and defects in the parts. Consequently, the defects noticeable in the printed parts do not only result from the photopolymerisation of the network, but also result from the way the parts were processed, i.e. from the rheological behaviour of the pastes.

Moreover, the thermal degradation cycles presented in Figs. 7 and 8

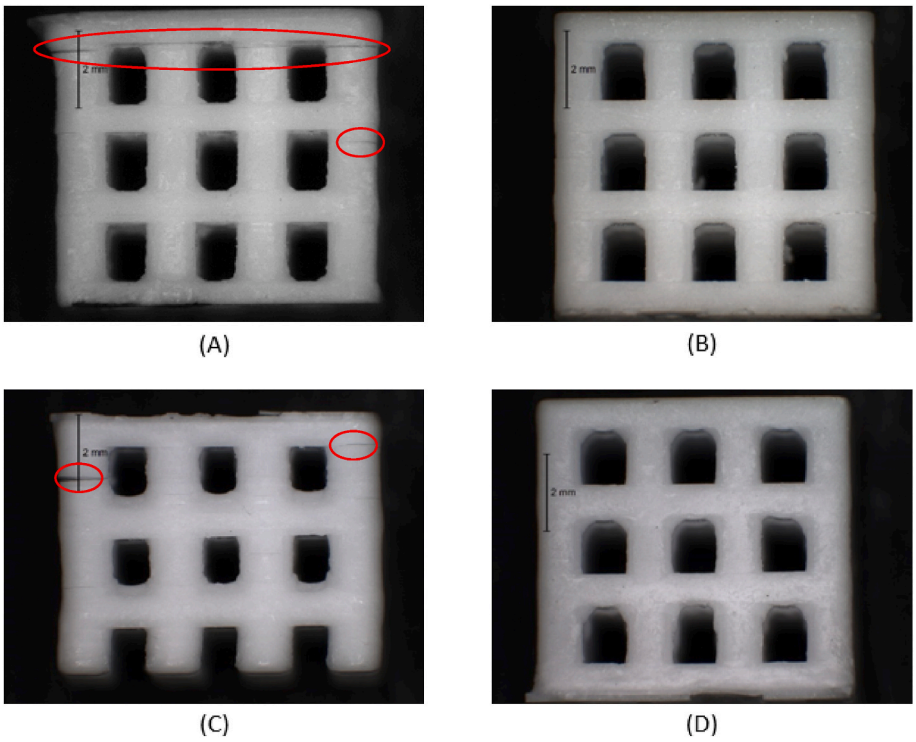

Fig. 13. Sintered parts, I1 (A), I2 (B), I3 (C) and I4 (D); red circles highlight the most visible cracks and delaminations. (For interpretation of the references to colour in this figure legend, the reader is referred to the Web version of this article.)

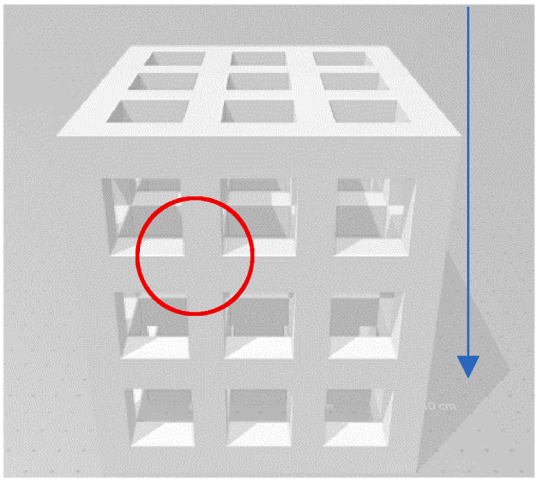

Fig. 14. Image showing the zone of the printed parts observed with the SEM (red circle); Blue arrow = printing direction. (For interpretation of the references to colour in this figure legend, the reader is referred to the Web version of this article.)

also showed differences between the samples depending on their composition. It appeared that the addition of HDDA to TGDA in the resin induced a slow thermal degradation of around 2.4 wt% of photo-cured polymer between 100 °C and 300 °C. Then, the addition of PEG 200 led to a modification of the thermal degradation of the photopolymer network with the elimination 5.0 wt% of polymer before 300 °C. In their study, S. Jiang et al. [36], explained that the thermal stability of a polymer network increased with the increase of functional groups bringing a higher crosslink density. On the other hand, Badev et al. [35] showed that diluents can reduce the overall functionality of a resin. Indeed, in the present study, with the addition of HDDA and PEG 200, the tetrafunctional diacrylate TGDA is replaced by a simple diacrylate and a non-reactive component. Therefore, the reduction of the number of functions in the network could lead to a thermally less stable photo-cured polymer, explaining at the same time the slow thermal degradation between 100 °C and 300 °C.

The composition of the resin was not the only parameter influencing the thermal degradation behaviour of cured pastes. As shown in Figs. 7 and 8, the light curing parameters also influenced the thermal degradation of the samples. Chartier et al. evaluate the influence of the irradiance ($W.cm^{-2}$) of the light source on the final samples and stipulate that increasing the irradiance leads to higher rates of polymerisation [16]. Therefore, a hypothesis is that a higher amount of energy (Fig. 10) leads to a thermally more stable network (due to the high polymerisation rate), whereas a lower amount of energy (Fig. 11) leads to a thermally less stable network and enables a slow thermal degradation in the first degrees. This might be a way to ease the debinding, explaining the presence of thinner defects after sintering in the parts cured with the lowest amount of energy (Figs. 9, 13 and 14).

In order to treat all the samples with the same thermal debinding cycle and considering that a maximum of 3 mass loss zones have been observed in the thermal degradation pattern, three holding temperatures were chosen for each mass loss. Then, the heating rate was chosen low: 0.5 °C/min to avoid defects formation in the part [18,37], and considering that for all the resin composition the organic phase was removed after 510 °C, the heating rate was increased to 3 °C/min from this temperature to 1100 °C. The chosen sintered temperature enabled a good sintering of the β-TCP and avoided the transformation from β to α-TCP [18] which was confirmed by XRD analysis.

5. Conclusion

The objective of this work was to highlight the influence of the resin composition on the printability of an array of tricalcium phosphate pastes with a DLP stereolithography machine. It was shown that the monomers enabling the preparation of a paste with the lowest viscosity, the best printability and the smoothest thermal degradation are TGDA,

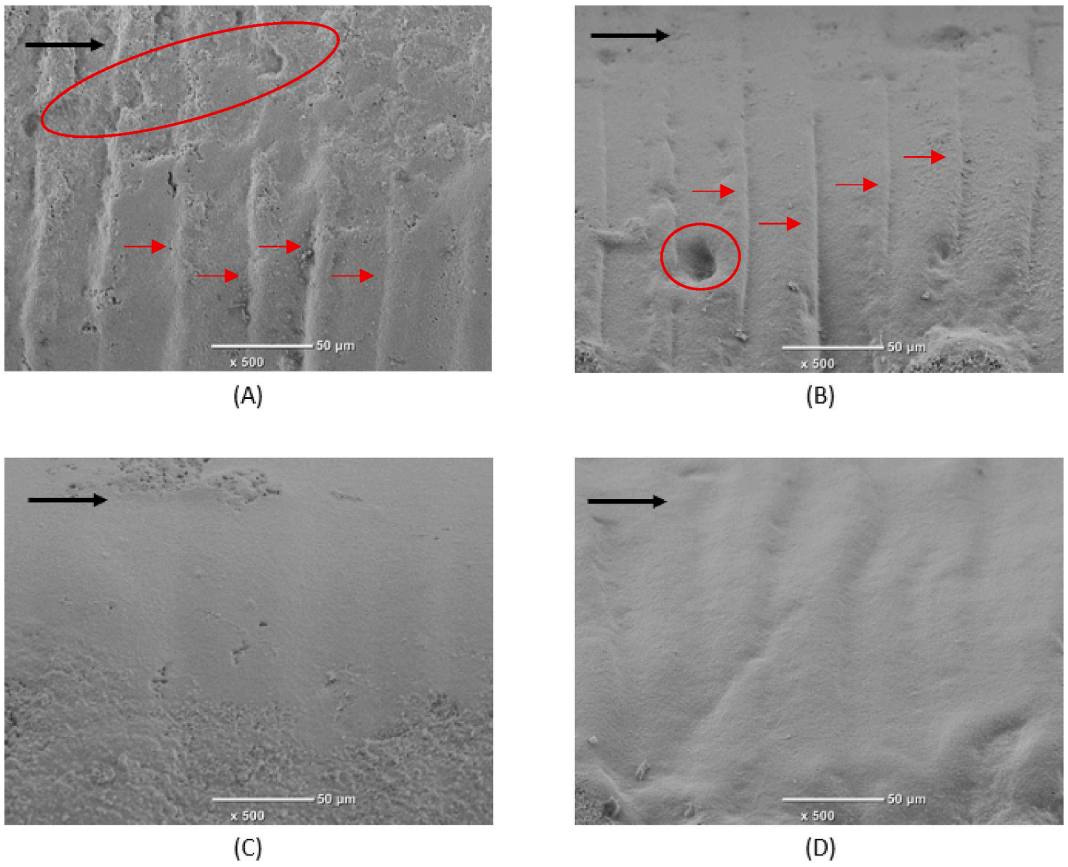

Fig. 15. SEM images of the sintered parts (×500), I1 (A), I2 (B), I3 (C) and I4 (D) defects = red circle and red arrows. (For interpretation of the references to colour in this figure legend, the reader is referred to the Web version of this article.)

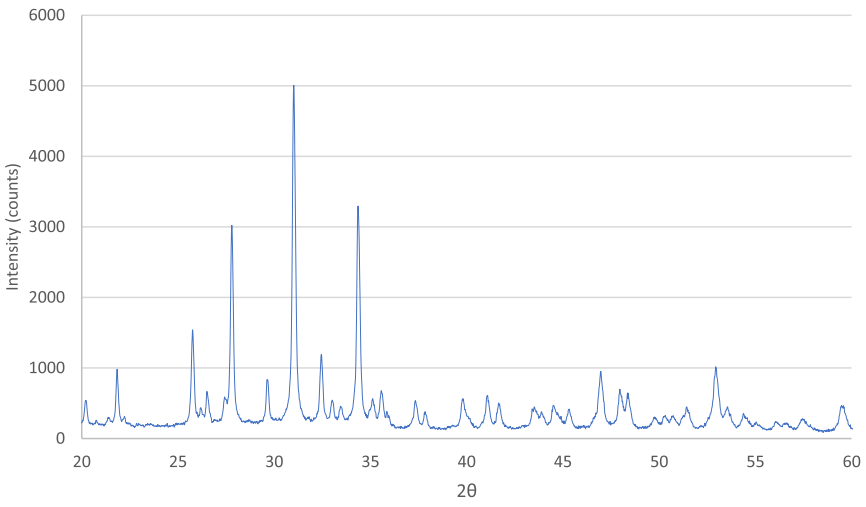

Fig. 16. XRD diagram highlighting peaks corresponding to the β-TCP phase according to the ICDD (International Center for Diffraction Data) [3].

HDDA, and PEG 200. Using these monomers and a β-TCP powder treated with 5 wt% of dispersant, pastes with 47 vol% of powder were prepared and printed. Tailoring the composition of the resin and reducing the light power during the building process enabled to have a better resolution of the green parts and less defects in the sintered objects. These results are encouraging for further development in order to finally obtain defect-free parts. The improving of the cleaning of the parts and the debinding cycle are interesting ideas to pursue the work and enhance the quality of the printed parts.

Declaration of competing interest

The authors declare that they have no known competing financial interests or personal relationships that could have appeared to influence the work reported in this paper.

Acknowledgments

The author is grateful to the “Doc 3D printing” project for financial support. This project has received funding from the European Union’s Horizon 2020 research and innovation program under the Marie Skłodowska-Curie grant agreement No 764935.

References

[1] Z. Xing, W. Liu, Y. Chen, W. Li, Effect of plasticizer on the fabrication and properties of alumina ceramic by stereolithography-based additive manufacturing, nov, Ceram. Int. 44 (16) (2018) 19939–19944, https://doi.org/10.1016/j.ceramint.2018.07.259.

[2] F.P.W. Melchels, J. Feijen, D.W. Grijpma, A review on stereolithography and its applications in biomedical engineering, août, Biomaterials 31 (24) (2010) 6121–6130, https://doi.org/10.1016/j.biomaterials.2010.04.050.

[3] S. Bose, M. Roy, A. Bandyopadhyay, Recent advances in bone tissue engineering scaffolds, oct, Trends Biotechnol. 30 (10) (2012) 546–554, https://doi.org/10.1016/j.tibtech.2012.07.005.

[4] E. Rguiti-Constantin, Frittage, propriétés mécaniques et fonctionnalisation de biocéramiques mono et biphasique, Université de Valencienne et du Hainaut-Cambrésis, 2011.

[5] R.Z. Legeros, S. Lin, R. Rohanizadeh, D. Mijares, et J.P. Legeros, « Biphasic Calcium Phosphate Bioceramics: Preparation, Properties and Applications », Elsevier, vol. vol. 14, p. 201-209.

[6] C. Schmidleithner, S. Malferrari, R. Palgrave, D. Bomze, M. Schwentenwein, D. M. Kalaskar, Application of high resolution DLP stereolithography for fabrication of tricalcium phosphate scaffolds for bone regeneration, jun, Biomed. Mater. 14 (4) (2019), 045018, https://doi.org/10.1088/1748-605X/ab279d.

[7] E. Johansson, O. Lidström, J. Johansson, O. Lyckfeldt, E. Adolfsson, Influence of resin composition on the defect formation in alumina manufactured by stereolithography, févr, Materials 10 (2) (2017) 138, https://doi.org/10.3390/ma10020138.

[8] Admatec introduces bioresorbable ceramics from CAM Bioceramics, Admatec (2020) consulté le déc. 17, https://admateceurope.com/news-item?id=89f1850704361acfa22bfcfd3b83be05.

[9] Y. Mingxian, et al., Optimization of the tape casting process for development of high performance alumina ceramics, Elsevier Ceram. Int. 41 (2015) 14845–14853.

[10] C.-J. Bae, J.W. Halloran, Influence of residual monomer on cracking in ceramics fabricated by stereolithograpy, Appl. Ceram. Technol. Ceram. Prod. Dev. Commer. 8 (2011) 1289–1295, https://doi.org/10.1111/j.1744-7402.2010.02578.x.

[11] M. Pfaffinger, M. Hartmann, M. Schwentenwein, J. Stampfl, Stabilization of tricalcium phosphate slurries against sedimentation for stereolithographic additive manufacturing and influence on the final mechanical properties, Int. J. Appl. Ceram. Technol. 14 (4) (2017) 499–506, https://doi.org/10.1111/ijac.12664.

[12] X. Song, Y. Chen, T. Woo Lee, S. Wu, L. Cheng, Ceramic fabrication using Mask-Image-Projection-based Stereolithography integrated with tape-cating, J. Manuf. Process. (2015) 456–464.

[13] J.W. Halloran, Ceramic stereolithography: additive manufacturing for ceramics by photopolymerization, juill, Annu. Rev. Mater. Res. 46 (1) (2016) 19–40, https://doi.org/10.1146/annurev-matsci-070115-031841.

[14] G. Mitteramskogler, et al., Light Curing Strategies for Lithography-Based Additive Manufacturing of Customized Ceramics, sept, Elsevier, 2014, https://doi.org/10.1016/j.addma.2018.08.003.

[15] S. Zürcher et, T. Graule, Influence of dispersant structure on the rheological properties of highly-concentrated zirconia dispersions, mar, J. Eur. Ceram. Soc. 25 (6) (2005) 863–873, https://doi.org/10.1016/j.jeurceramsoc.2004.05.002.

[16] T. Chartier, et al., Influence of irradiation parameters on the polymerization of ceramic reactive suspensions for stereolithography, déc, J. Eur. Ceram. Soc. 37 (15) (2017) 4431–4436, https://doi.org/10.1016/j.jeurceramsoc.2017.05.050.

[17] K. Kowsari, et al., Photopolymer formulation to minimize feature size, surface roughness, and stair-stepping in digital light processing-based three-dimensional printing, Addit. Manuf. 24 (déc. 2018) 627–638, https://doi.org/10.1016/j.addma.2018.10.037.

[18] M. Lasgorceix, Mise en forme par microstéréolithographie et frittage de céramiques macro-micro-poreuses en hydroxyapatite silicatée et évaluation biologique, Université de Limoge, 2014, https://doi.org/10.13140/rg.2.1.1895.8484.

[19] T. Chartier, et al., Fabrication of millimeter wave components via ceramic stereo- and microstereolithography processes, J. Am. Ceram. Soc. (2008), https://doi.org/10.1111/j.1551-2916.2008.02482.x. ???-???, juin.

[20] V.K. Popov, A.V. Evseev, A.L. Ivanov, V.V. Roginski, A.I. Volozhin, S.M. Howdle, Laser stereolithography and supercritical fluid processing for custom-designed implant fabrication, févr, J. Mater. Sci. Mater. Med. 15 (2) (2004) 123–128, https://doi.org/10.1023/B:JMSM.0000011812.08185.2a.

[21] J. Schmidt, P. Colombo, Digital light processing of ceramic components from polysiloxanes, janv, J. Eur. Ceram. Soc. 38 (1) (2018) 57–66, https://doi.org/10.1016/j.jeurceramsoc.2017.07.033.

[22] J. Kindernay, A. Blažková, J. Rudá, V. Jančovičová, Z. Jakubíková, Effect of UV light source intensity and spectral distribution on the photopolymerisation reactions of a multifunctional acrylated monomer, août, J. Photochem. Photobiol. Chem. 151 (1–3) (2002) 229–236, https://doi.org/10.1016/S1010-6030(02)00172-7.

[23] B. Steyrer, P. Neubauer, R. Liska, J. Stampfl, Visible light photoinitiator for 3D-printing of tough methacrylate resins, déc, Materials 10 (12) (2017) 1445, https://doi.org/10.3390/ma10121445.

[24] K. Li, Z. Zhao, The effect of the surfactants on the formulation of UV-curable SLA alumina suspension, avr, Ceram. Int. 43 (6) (2017) 4761–4767, https://doi.org/10.1016/j.ceramint.2016.11.143.

[25] S.C. Ligon, R. Liska, J. Stampfl, M. Gurr, R. Mülhaupt, Polymers for 3D printing and customized additive manufacturing, août, Chem. Rev. 117 (15) (2017) 10212–10290, https://doi.org/10.1021/acs.chemrev.7b00074.

[26] M. Descamps, J.C. Hornez, A. Leriche, Effects of powder stoichiometry on the sintering of β-tricalcium phosphate, janv, J. Eur. Ceram. Soc. 27 (6) (2007) 2401–2406, https://doi.org/10.1016/j.jeurceramsoc.2006.09.005.

[27] N. Somers, F. Jean, M. Lasgorceix, H. Curto, G. Urruth, A. Thuault, F. Petit, A. Leriche, et al., Influence of dopants on thermal stability and densification of β-tricalcium phosphate powders, Open Ceram. 7 (2021) 1–13, https://doi.org/10.1016/j.oceram.2021.100168.

[28] M. Ebrahimi, M. Botelho, Biphasic calcium phosphates (BCP) of hydroxyapatite (HA) and tricalcium phosphate (TCP) as bone substitutes: importance of physicochemical characterizations in biomaterials studies, févr, Data Brief 10 (2017) 93–97, https://doi.org/10.1016/j.dib.2016.11.080.

[29] B. Bitterlich, C. Lutz, A. Roosen, Rheological Characterization of Water-Based Slurries for the Tape Casting Process, 6th, 28, Ceramics International, 2002, pp. 675–683.

[30] T. Chartier, A. Badev, Y. Abouliatim, P. Lebaudy, L. Lecamp, Stereolithography process: influence of the rheology of silica suspensions and of the medium on polymerization kinetics – cured depth and width, juill, J. Eur. Ceram. Soc. 32 (8) (2012) 1625–1634, https://doi.org/10.1016/j.jeurceramsoc.2012.01.010.

[31] S. Mueller, E.W. Llewellin, H.M. Mader, « the rheology of suspensions of solid particles », Art. no 2116, avr, Proc. R. Soc. Math. Phys. Eng. Sci. 466 (2116) (2010), https://doi.org/10.1098/rspa.2009.0445.

[32] V. Tomeckova, F. Teyssandier, S.J. Norton, B.J. Love, J.W. Halloran, Photopolymerization of acrylate suspensions, nov, J. Photochem. Photobiol. Chem. 247 (2012) 74–81, https://doi.org/10.1016/j.jphotochem.2012.08.008.

[33] E. Andrzejewska, Photopolymerization kinetics of multifunctional monomers, mai, Prog. Polym. Sci. 26 (4) (2001) 605–665, https://doi.org/10.1016/S0079-6700(01)00004-1.

[34] C. Decker, Polymérisation Sous Rayonnement UV, 2000, p. 19.

[35] A. Badev, et al., Photopolymerization kinetics of a polyether acrylate in the presence of ceramic fillers used in stereolithography, juill, J. Photochem. Photobiol. Chem. 222 (1) (2011) 117–122, https://doi.org/10.1016/j.jphotochem.2011.05.010.

[36] S. Jiang, et al., Photopolymerization of multifunctional methacrylic monomers: synthesis, properties and effects of the functional groups, J. Polym. Mater. (2016) 11.

[37] S. Md Ani, A. Muchtar, N. Muhamad, J.A. Ghani, Binder removal via a two-stage debinding process for ceramic injection molding parts, Art. no 2, mars, Ceram. Int. 40 (2) (2014), https://doi.org/10.1016/j.ceramint.2013.10.032.